PROCEEDINGS, 49th Workshop on Geothermal Reservoir Engineering
Stanford University, Stanford, California, February 12-14, 2024
SGP-TR-227

Including Permeability Anisotropy in Fault Zones Models Helps Coping with Both Geothermal Reservoir Storage Estimation and Induced Seismicity

Nicolas Wynants-Morel, Jeanne Vidal and David Soubeyrand

Lithium de France, 16 rue des Couturières, 67240 Bischwiller, France

nicolas.wynants@lithiumdefrance.com

Keywords: geomechanical modeling, Upper Rhine Graben, fractured porous media, reservoir storage, induced seismicity

ABSTRACT

Lithium de France is the first independent French operator that aims to extract heat and geothermal lithium. Their project consists in producing hot and Li-rich fluid naturally circulating inside a fracture network in the Upper Rhine Graben. Nonetheless, previous geothermal projects have highlighted the highly seismogenic nature of the faults system in this region. Therefore, mitigating the seismic risk related to deep geothermal exploitation and anticipating reservoir development is essential for the project of Lithium de France.

Using the subsurface knowledge acquired during geophysical exploration campaigns, a thermo-hydro-geomechanical model has been built with the 2D finite element code Disroc. The fault zones have been divided into a discrete core zone, and an inner and an outer damage zone, represented as equivalent continuous formations. Cold fluid is injected inside the outer damage zone of a major fault zone, near 2000 meters depth. The open-hole section of the production well is located 1.2km away from the injection point at a similar depth within the fault damage zone (FDZ).

In order to evaluate the reservoir storage capacity and the risks of fault reactivation, 2 ranges of permeability for the fault zones have been compared: a large permeability case and a low permeability case. The case with the largest permeability shows small fluid pressure variations (less than 20 bars after 20 years of fluid circulation), with productivity and injectivity indexes observed in similar geothermal projects such as the neighbor project of Rittershoffen. In the low permeability case, induced seismicity is expected at a similar flowrate after a few years, as observed in such geothermal projects. Therefore, a permeability anisotropy must be considered in fault zones, to account for both the storage and the geomechanical aspects of the geothermal fault reservoir.

1. INTRODUCTION

Various geological studies and measurements from previously drilled geothermal projects in Northern Alsace showed geothermal gradient anomalies, with up to 150°C at 1500 meters depth (Baillieux et al., 2013; Pribnow and Schellschmidt, 2000), but also high lithium concentration in the brine circulating in the faulted crystalline basement (Aquilina et al., 1997; Kölbel et al., 2023; Sanjuan et al., 2016). Lithium de France is the first independent French geothermal operator linking in a same project the two following aspects: (1) producing direct heat from the geothermal brine circulating inside the fracture network in the Upper Rhine Graben; and (2) extracting battery-grade lithium from this brine, with a minimal environmental impact.

Lithium de France already owns 2 geothermal exploration licenses in Northern Alsace, called Les Sources and Les Poteries, and 1 lithium mining exploration license, called Les Sources Alcalines (Fig 1). To improve the subsurface knowledge of these areas, geophysical exploration campaigns (two 3D seismic campaigns and a Controlled Source Electro-Magnetic, or CSEM, acquisition) were performed in 2022 and 2023 on these exploration licenses to better characterize the subsurface structures and their tendency to fluid storage (Fig 1). Moreover, Lithium de France acquired and reprocessed vintage 2D lines to improve 3D seismic data processing and interpretation, with the help of geological and geophysical data from neighboring wells (Fig 1). A 3D geological static model was built on the Leapfrog software (Seequent) from five seismic horizons and multiple fault signatures converted to depth, to 3D visualize the geothermal reservoir.

Previous geothermal experiences in the Upper Rhine Graben show geomechanical instability of the faults and fractures present in the reservoirs, with generation of induced microseismicity during geothermal activities (Baujard et al., 2020; Schmittbuhl et al., 2021). Therefore, the estimation of seismic risk through fault reactivation must be modeled to estimate the viability of the geothermal exploitation, besides reservoir modeling of the resource. Moreover, the fracture system composing the faults' damage zone results in permeability heterogeneities in the reservoir (Llanos et al., 2015; Malin et al., 2020; Panja et al., 2021), which impact local pressure and thus induced seismicity triggering (Khajehdehi et al., 2022). In order to make previsional estimations of both hot fluid storage in the reservoir and geomechanical issues, we built a thermo-hydro-mechanical model using the 2D Disroc code (Pouya, 2016). As no well has been drilled in the considered exploration licenses yet, we consider a simple model to overcome the lack of information about the faults mechanical properties and connectivity in depth and yet to have a global estimation of the reservoir behavior.

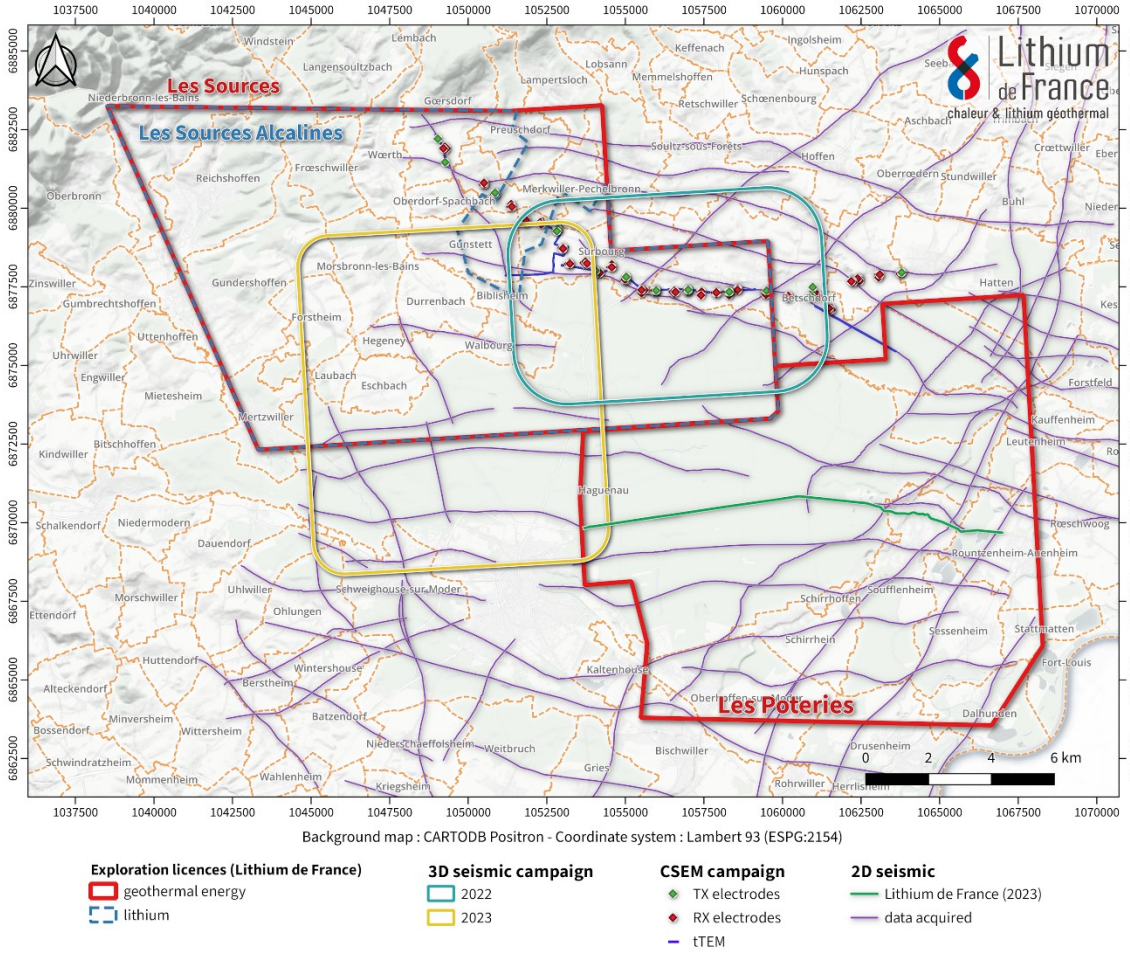

Figure 1: Exploration licenses and geophysical data

2. PREDICTIVE DYNAMIC MODELLING

2.1 Short Description of the Numerical Code

Disroc is a 2D THM finite-element software for modelling mechanical deformation and thermal and hydraulic processes in fractured rock masses. It is designed to support discontinuities such as deterministic faults and DFN (Discrete Fracture Network).

The main equations governing the THM processes used in Disroc are described below. Details can be found in Pouya (2016). Fluid is considered incompressible and flows in the continuous matrix and throughout the discrete faults, both saturated. In the porous rock matrix, the flow is governed by Darcy's law. Combining Darcy's law for linear fluid flow with the fluid mass conservation law, hydraulic diffusion is given in the matrix by:

$$C_M \frac{\partial P}{\partial t} = \mathrm{div}(\bar{\bar{k}} \nabla \Psi) \tag{1}$$

where P is the fluid pressure (Pa), C_M the compressibility coefficient (Pa^{-1}), k the permeability tensor (m^2), $\Psi = P + \gamma_f z$ the hydraulic head (Pa), $\gamma_w = g\rho_w$ the fluid density (Pa/m) where ρ_w the fluid density ($kg.m^{-3}$) and g the gravity intensity ($m.s^{-2}$). ∇ and div are the gradient and divergent operators, respectively. The notation $\bar{\bar{.}}$ refers to a tensor.

Concerning fluid flow in fractures, the following equation ensures fluid mass balance along the interface:

$$C_{Mf} \frac{\partial P}{\partial t} = \nabla_s . (c_f \bar{v}) - [\![\bar{v}]\!] . \bar{n} \tag{2}$$

where C_{Mf} is the fracture compressibility coefficient (Pa^{-1}), c_f the fracture hydraulic conductivity, v the fluid velocity and n the normal to the interface plane (-). ∇_s represents the tangent gradient in the local plane of the interface, $[\![.]\!]$ refers to the discontinuity of the considered property at the interface. The notation $\bar{.}$ refers to a vector.

Even though the code manages thermal advection, we consider heat transfer only through conduction here, using Fourier's law of heat transport:

$$\overline{w} = -\overline{\overline{\lambda}}\nabla T \tag{3}$$

where w is the heat flow ($W.m^{-2}$), λ the heat conductivity tensor ($W.m^{-1}.K^{-1}$) and T the temperature (K).

The thermal energy balance is given by:

$$C_T \frac{\partial T}{\partial t} = -\mathrm{div}(\overline{w}) \tag{4}$$

where C_T is the thermal capacity ($J.kg^{-1}.K^{-1}$).

The geomechanical behavior of rock masses and discontinuities can be elastic or elasto-plastic. We consider here linear thermo-poro-elasticity in rock matrix, with the stiffness tensor relating the stress tensor to the strain tensor through generalized Hooke's law.

We consider discontinuities to adopt elastic linear behavior in normal direction, elastic and then perfectly plastic behavior in shear direction. Plastic shear stress limited by the fracture shear strength expressed in the Mohr plane by the Mohr-Coulomb failure criterion:

$$\sqrt{\tau^2} - \mu\sigma_N^{eff} - C = 0 \tag{5}$$

where τ is the shear stress (Pa), $\sigma_N^{eff} = \sigma_N - P$ the effective normal stress (Pa), σ_N the normal stress (Pa), μ the friction coefficient (-) and C the cohesion (Pa).

The increment of shear plastic displacement is derived from a non-associated plastic flow relation:

$$\Delta u^p = \lambda_p \frac{\partial G}{\partial \tau} \tag{6}$$

where Δu^p is the increment of shear plastic displacement (m), λ_p the plastic multiplier (-), $G = \sqrt{\tau^2} - \sigma_N^{eff} \tan\varphi_0$ the plastic potential (Pa) and φ_0 the dilatancy angle (°).

2.2 Conceptual Model

The geothermal reservoir is defined as an assembly of porous and fractured sedimentary formations and faulted granitic basement, in accordance with the literature from the neighbor geothermal projects (Baujard et al., 2017; Degouy et al., 1992; Reinecker et al., 2019). The fault zones are divided in an outer damage zone (ODZ), with a low fracture intensity, altered and more permeable than the surrounding rock; an inner damage zone (IDZ), with a higher fracture intensity, more altered and more permeable than the ODZ; and a fault plane, where most of the fault displacement occurs (Figure 2 and Figure 3). In accordance with the observations from the wells from the Soultz and Rittershoffen projects (Dezayes et al., 2010; Sausse and Genter, 2005; Vidal et al., 2017, 2016), and relationships between fault offset and damage zone width at outcrop scale (Torabi et al., 2020), the faults are divided in 3 types with associated damage zone width detailed in Table 1. The fault planes are considered discrete while the damage zones are represented as equivalent continuous materials (Cappa, 2011; Rinaldi et al., 2014), only represented in the hanging wall block, in accordance with well data from a neighboring project (Vidal et al., 2017).

The 2D constructed model is defined as a horizontal slice of the 3D geological model to estimate the global behavior of the reservoir, including fault connections (Figure 3). The intact rock matrix in this 2D model represents an equivalent reservoir. Therefore, its thermo-hydro-mechanical properties are averaged by the heights of the different rock formations forming the reservoir. The geothermal exploitation is expected to present a single well doublet. These wells are represented as 2 source points, located at the intersection between the well trajectories and the model plane. These points appear to be in a fault outer damage zone.

We choose to consider a simplified model with no thermal advection. Nonetheless, we consider a thermal pseudo-advection, with the thermal properties of the fault zones being function of the hydraulic conductivities of these zones. Fault failure occurs when a simplified Mohr-Coulomb criterion is reached (Equation 5), with a null cohesion and a friction coefficient of 1, in accordance with the literature (Cornet et al., 2007). In order to better understand the evolution of the geomechanical behavior of faults during fluid circulation, the Coulomb Failure Stress, or CFS, has been computed for each fault segment in our model:

$$CFS = \sqrt{\tau^2} - \sigma_N^{eff} \tag{7}$$

To account for water reinjection related to the lithium extraction process, the injection flowrate is considered higher than the production flowrate. The percentage of overinjected fluid is fixed and has been determined to limit reactivation of neighbor faults and microseismicity triggering.

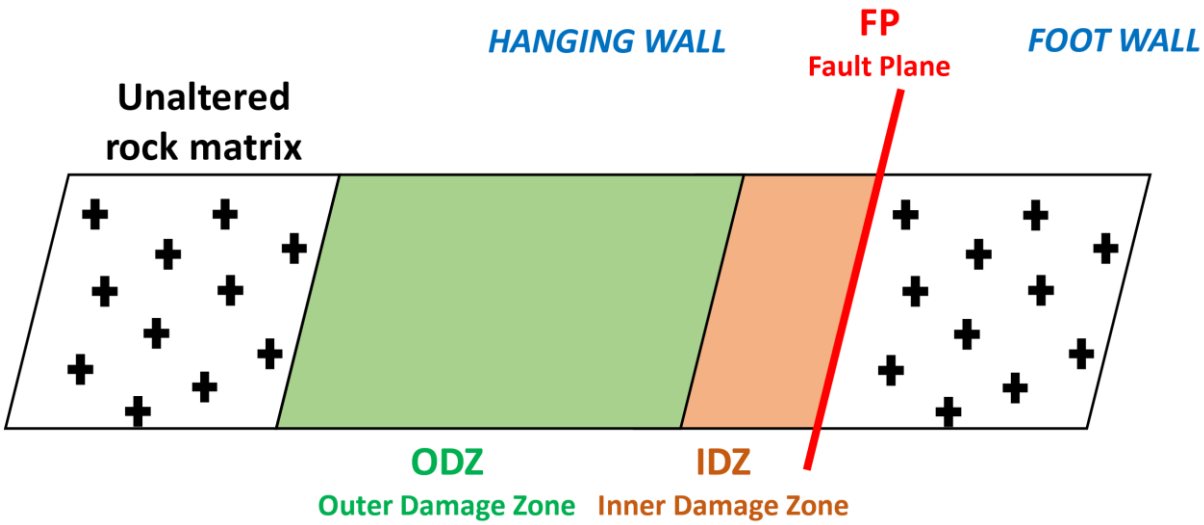

Figure 2: Conceptual model adopted for fault zones

Table 1 : Size characteristics of the faults' damage zones

	Type 1 faults	Type 2 faults	Type 3 faults
Main orientation	Mostly N-S	Variable	Variable
Fault offset estimated with the 3D seismic cube (m)	200	50	10
Width of the ODZ (m)	150	40	10
Width of the IDZ (m)	50	10	1

2.3 Model Setup: Geometry, Initial Conditions, and Thermo-Hydro-Mechanical Properties

The model is located at 2 kilometers depth, that is in the granitic basement according to the 3D seismic imaging and the neighboring geothermal wells (Aichholzer et al., 2016; Duringer et al., 2019). It consists of a 7 km-per-10 km studied zone embodied in a 40 km-per-50 km area (Figure 3a). The continuous formations are considered homogeneous, isotropic, permeable, and linearly elastic.

The initial pressure, temperature and stress state are assumed homogeneous on the model and in accordance with the literature on the Upper Rhine Graben (Guillou-Frottier et al., 2013; Valley and Evans, 2007) (Table 2). The adopted thermo-hydro-mechanical properties of the rocks and faults are summarized in Table 3, in accordance with the literature on the hydraulic tests from the Upper Rhine Graben geothermal projects (Azzola et al., 2019; Cornet et al., 2007; GeORG Team, 2013; Kushnir et al., 2018; Mahmoodpour et al., 2021; Rachez and Gentier, 2010; Stober and Bucher, 2015). Equivalent thermal properties are considered due to pseudo-advection. The production flowrate is constant and equal to 250 m^3/h. The reinjection temperature is equal to 64°C. 20 years of fluid circulation are simulated.

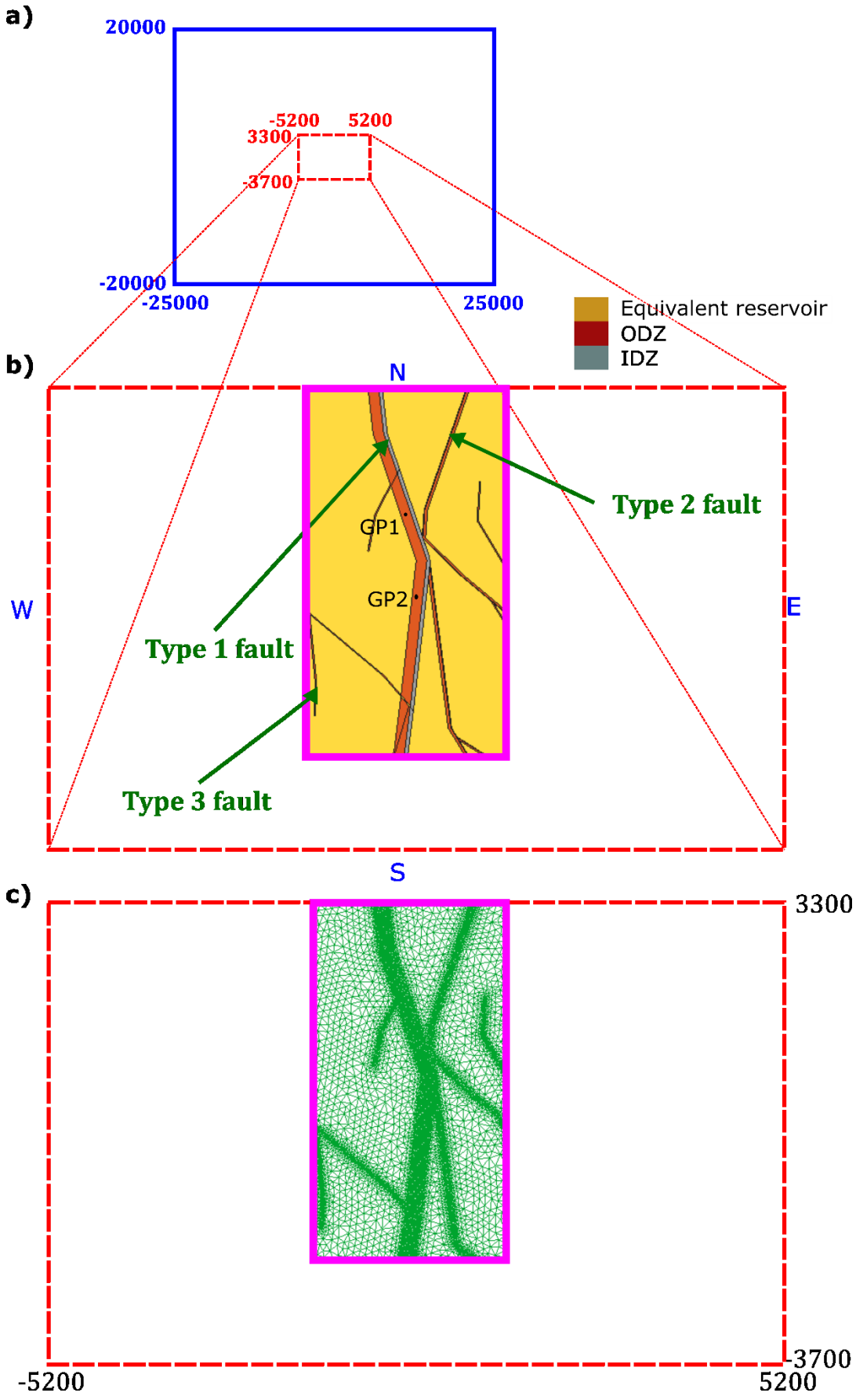
a)
20000
-5200
5200
3300
-3700
-20000
-25000
25000
Equivalent reservoir
ODZ
IDZ
b)
N
W
E
S
GP1
GP2
Type 1 fault
Type 2 fault
Type 3 fault
c)
3300
-3700
-5200
5200

Figure 3: Conceptual representation and meshing of the model. For confidentiality reasons, the static model is detailed within the pink zone only.

Table 2: Thermal, hydraulic and mechanical initial conditions used in the model

Parameters	Value
Initial temperature T_0 (°C)	144
Initial fluid pressure P_0 (bar)	205
Initial maximal horizontal stress S_{Hmax} (MPa)	47.2
Initial minimal horizontal stress S_{hmin} (MPa)	26.8
Initial vertical stress[1] S_v (MPa)	49.7

Table 3: Thermal, hydraulic and mechanical properties used in the model. Values in italic are used in the low permeability case, values in bold in the high permeability case.

	Equivalent reservoir	ODZ	IDZ	Fault plane
Equivalent thermal conductivity λ (W/m/K)	5.93	**108** *56*	**150** *79.2*	42.5
Equivalent specific heat capacity C_T (J/kg/K)	447	**46** *57.1*	**32.8** *40.4*	74.1
Linear thermal expansion coefficient α_T (1/K)	1.4E-5			
Intrinsic permeability k (m^2)	1.3E-15	**1.15E-11** *2.3E-12*	**4.65E-11** *9.3E-12*	7.5E-13
Porosity Φ (%)	3.5	4.8	9.3	100
Storativity S (1/Pa)	6.81E-10	1.06E-9	2.66E-9	4.54E-10
Biot coefficient b (-)	0.24	0.5	0.5	1
Dilation angle φ_0 (°)	-	-	-	5
Young modulus E (GPa)	52	39	7	-
Poisson ratio ν (-)	0.26	0.26	0.26	-
Density ρ (kg/m3)	2.7	2.7	2.7	-
Normal stiffness k_N (GPa/m)	-	-	-	40
Shear stiffness k_S (GPa/m)	-	-	-	4
Friction coefficient μ (-)	-	-	-	1
Cohesion C (MPa)	-	-	-	0

[1] Even though the vertical direction is not represented in the model, vertical stress is still considered.

3. INFLUENCE OF THE PERMEABILITY OF FAULT ZONES

We compare 2 ranges of fault zone permeabilities (Table 3) in terms of pressure, temperature and stress variations in the reservoir.

3.1 Reservoir storage estimation

Figure 4 shows pressure and temperature variations after 20 years of fluid circulation for both damage zone permeability models. In the low damage zone permeability model, a very high overpressure (near 100 bars) is observed close to the injection well after 20 years of fluid circulation (Figure 4-a). In the high damage zone permeability, the overpressure is far lower, with near 20 bars at the injection well after 20 years (Figure 4-b) ; this value is in accordance with other EGS numerical simulations in the Upper Rhine Graben (Goldberg et al., 2023).

No significant temperature decrease has been observed at production well after 20 years of circulation in both cases (Figures 4-c and 4-d). Nonetheless, the size of the temperature drop zone is higher in the high permeability case than in the low permeability case, as expected with thermal pseudo-advection. Therefore, the temperature starts decreasing at the production well before 20 years of fluid circulation in the high permeability case, with a thermal drop of 4°C being observed after 20 years of fluid circulation. We have to note that the symmetrical behavior of the thermal response of the models is an artifact related to the pseudo-advection.

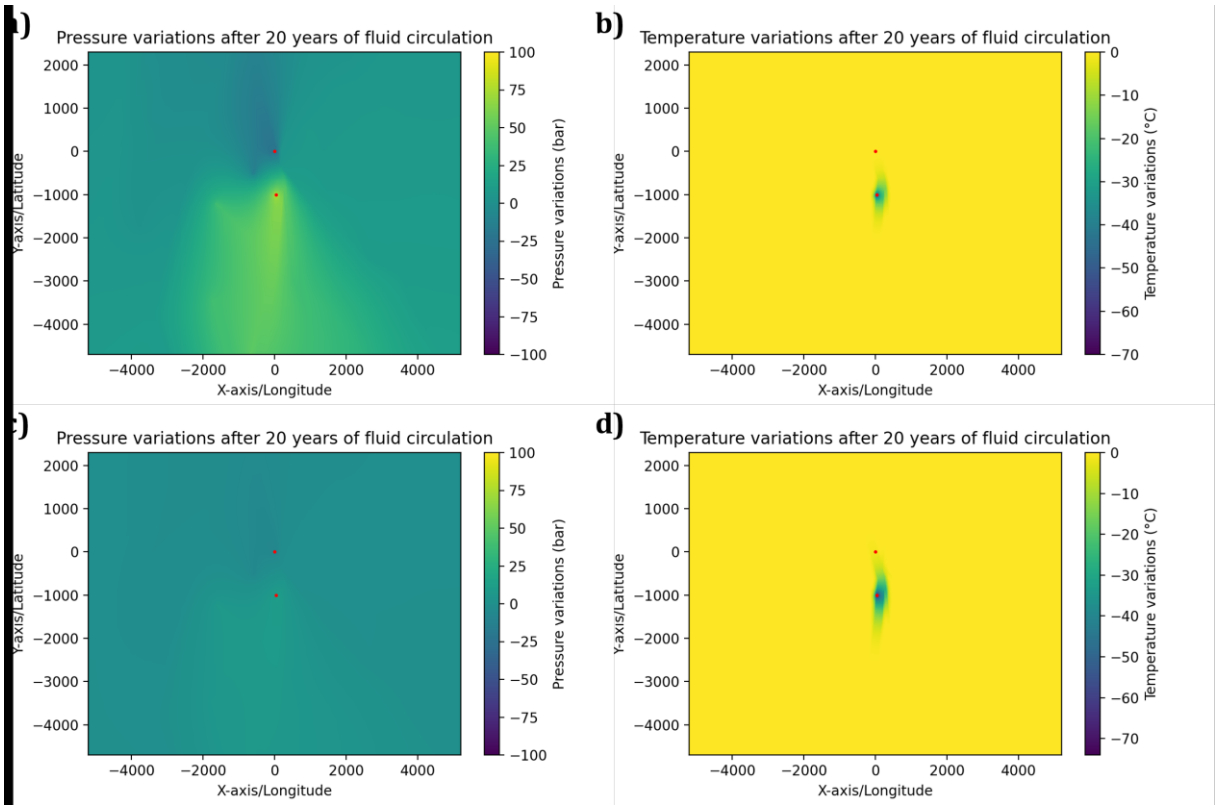

Figure 4: Fluid pressure and temperature variations after 20 years of fluid circulation in (a,b) low and (c,d) high damage zone permeability cases

3.2 Fault reactivation and potential induced seismicity

Figure 5 shows the proximity of reactivation of the faults represented in the model in both permeability cases, before exploitation and after 20 years of fluid circulation. Before geothermal exploitation, the stress state is critical with 73% of the faults' segments having a CFS less than 5 MPa. Rupture is expected in the high damage zone permeability case after 19 years of fluid circulation, whereas faults are reactivated after 5 years of fluid circulation in the low damage zone permeability case. In this particular case, possible induced microseismicity could occur near injection on a fracture sub-parallel to the near main fault after 3 years, as observed at the Rittershoffen exploitation, where an induced event with M_L>1.5 has been detected close to the geothermal operation after 2 years and 8 months of fluid circulation (Maurer et al., 2020)

4. CONCLUSION

We built 2D horizontal THM model to simulate the expected behavior of a geothermal reservoir in the Upper Rhine Graben. As no well data has been acquired by Lithium de France yet, we consider a simple model, with unilateral coupling (H->M, T->M), no thermal convection, a Mohr-Coulomb rupture criterion and a constant friction law. In this way, we have a rough estimation of both

storage and seismicity in the reservoir. Nonetheless, a separate set of hydraulic properties must be considered for each estimation, as both estimations require different kinds of concern. Another solution could be in considering permeability anisotropy in the fault zone, with stochastic repartition of permeability values. This may need a more complex model that can be built after well drilling and data acquisition from well tests and monitoring of induced microseismicity.

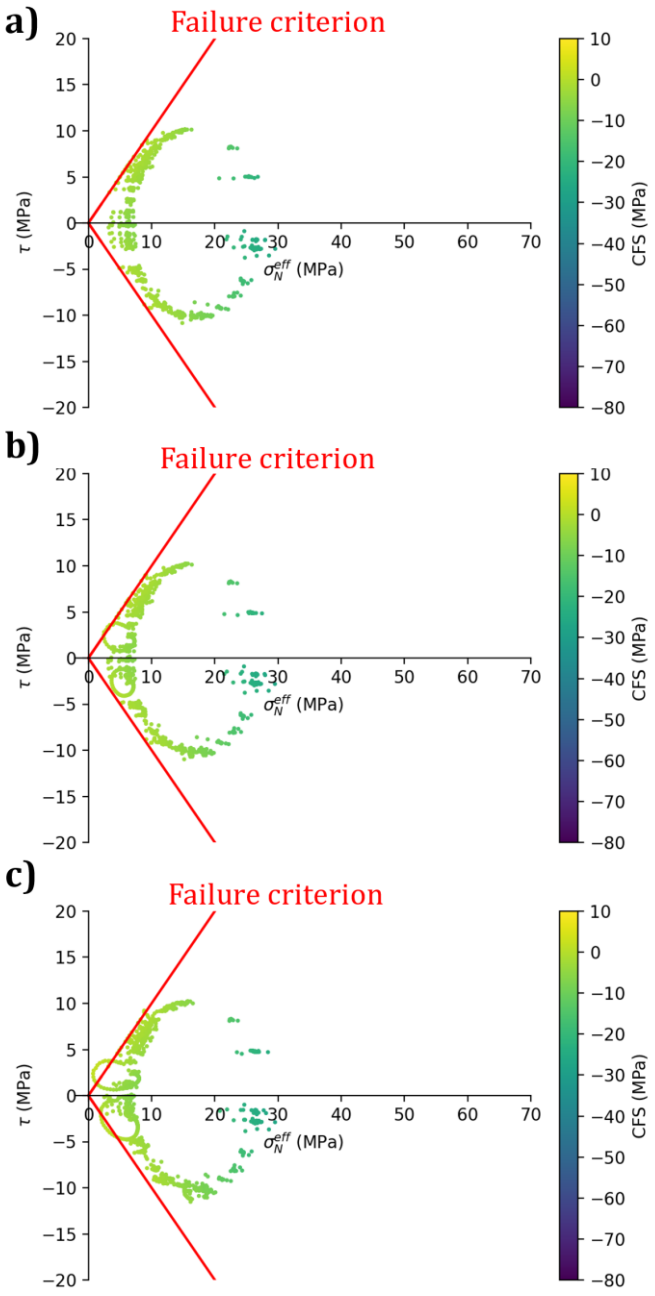

Figure 5: Proximity to failure of faults (a) before the beginning of the exploitation and after 20 years of fluid circulation in (b) high and (c) low damage zone permeability cases.

REFERENCES

Aichholzer, C., Duringer, P., Orciani, S., Genter, A., 2016. New stratigraphic interpretation of the Soultz-sous-Forêts 30-year-old geothermal wells calibrated on the recent one from Rittershoffen (Upper Rhine Graben, France). Geotherm. Energy 4, 1–26. https://doi.org/10.1186/s40517-016-0055-7

Aquilina, L., Pauwels, H., Genter, A., Fouillac, C., 1997. Water-rock interaction processes in the Triassic sandstone and the granitic basement of the Rhine Graben: Geochemical investigation of a geothermal reservoir. Geochim. Cosmochim. Acta 61, 4281–4295.

Azzola, J., Valley, B., Schmittbuhl, J., Genter, A., 2019. Stress characterization and temporal evolution of borehole failure at the Rittershoffen geothermal project. Solid Earth 10, 1155–1180. https://doi.org/10.5194/se-10-1155-2019

Baillieux, P., Schill, E., Edel, J.-B., Mauri, G., 2013. Localization of temperature anomalies in the Upper Rhine Graben: insights from geophysics and neotectonic activity. Int. Geol. Rev. 55, 1744–1762. https://doi.org/10.1080/00206814.2013.794914

Baujard, C., Cuenot, N., Maurer, V., Ravier, G., Seibel, O., Genter, A., Hehn, R., 2020. Geothermal operation feedback of the Soultz and Rittershoffen plants after 4 years of operations. Presented at the IGC Online Meeting.

Baujard, C., Genter, A., Dalmais, E., Maurer, V., Hehn, R., Rosillette, R., Vidal, J., Schmittbuhl, J., 2017. Hydrothermal characterization of wells GRT-1 and GRT-2 in Rittershoffen, France: Implications on the understanding of natural flow systems in the Rhine Graben. Geothermics 65, 255–268.

Cappa, F., 2011. Influence of hydromechanical heterogeneities of fault zones on earthquake ruptures: Fault hydromechanics and earthquake ruptures. Geophys. J. Int. 185, 1049–1058. https://doi.org/10.1111/j.1365-246X.2011.04994.x

Cornet, F., Bérard, T., Bourouis, S., 2007. How close to failure is a granite rock mass at a 5 km depth? Int. J. Rock Mech. Min. Sci. 44, 47–66.

Degouy, M., Villeneuve, B., Weber, R., 1992. Logistical support and development of the Soultz Hot Dry Rock site: seismic observation wells and well EPS-1, Final drilling report (No. RR-41179-FR). BRGM, Commission of European Communities, Bruxelles, Belgique.

Dezayes, C., Genter, A., Valley, B., 2010. Structure of the low permeable naturally fractured geothermal reservoir at Soultz. Comptes Rendus Geosci. 342, 517–530.

Duringer, P., Aichholzer, C., Orciani, S., Genter, A., 2019. The complete lithostratigraphic section of the geothermal wells in Rittershoffen (Upper Rhine Graben, eastern France): a key for future geothermal wells. Bull. Société Géologique Fr. 190, 13. https://doi.org/10.1051/bsgf/2019012

GeORG Team, 2013. Potentiel géologique profond du Fossé rhénan supérieur. Rapport final du projet GeORG – INTERREG IV – Partie 2 : géologie et potentiel (Rapport accessible en ligne).

Goldberg, V., Dashti, A., Egert, R., Benny, B., Kohl, T., Nitschke, F., 2023. Challenges and Opportunities for Lithium Extraction from Geothermal Systems in Germany—Part 3: The Return of the Extraction Brine. Energies 16, 5899. https://doi.org/10.3390/en16165899

Guillou-Frottier, L., Carré, C., Bourgine, B., Bouchot, V., Genter, A., 2013. Structure of hydrothermal convection in the Upper Rhine Graben as inferred from corrected temperature data and basin-scale numerical models. J. Volcanol. Geotherm. Res. 256, 29–49.

Khajehdehi, O., Karimi, K., Davidsen, J., 2022. The Effect of Correlated Permeability on Fluid-Induced Seismicity. Geophys. Res. Lett. 49, e2021GL095199. https://doi.org/10.1029/2021GL095199

Kölbel, L., Kölbel, T., Herrmann, L., Kaymakci, E., Ghergut, I., Poirel, A., Schneider, J., 2023. Lithium extraction from geothermal brines in the Upper Rhine Graben: A case study of potential and current state of the art. Hydrometallurgy 221, 106131. https://doi.org/10.1016/j.hydromet.2023.106131

Kushnir, A.R., Heap, M.J., Baud, P., Gilg, H.A., Reuschlé, T., Lerouge, C., Dezayes, C., Duringer, P., 2018. Characterizing the physical properties of rocks from the Paleozoic to Permo-Triassic transition in the Upper Rhine Graben. Geotherm. Energy 6, 1–32.

Llanos, E.M., Zarrouk, S.J., Hogarth, R.A., 2015. Numerical model of the Habanero geothermal reservoir, Australia. Geothermics 53, 308–319. https://doi.org/10.1016/j.geothermics.2014.07.008

Mahmoodpour, S., Singh, M., Turan, A., Bär, K., Sass, I., 2021. Hydro-Thermal Modeling for Geothermal Energy Extraction from Soultz-sous-Forêts, France. Geosciences 11, 464.

Malin, P.E., Leary, P.C., Cathles, L.M., Barton, C.C., 2020. Observational and Critical State Physics Descriptions of Long-Range Flow Structures. Geosciences 10, 50. https://doi.org/10.3390/geosciences10020050

Maurer, V., Gaucher, E., Grunberg, M., Koepke, R., Pestourie, R., Cuenot, N., 2020. Seismicity induced during the development of the Rittershoffen geothermal field, France. Geotherm. Energy 8, 1–31.

Panja, P., McLennan, J., Green, S., 2021. Impact of permeability heterogeneity on geothermal battery energy storage. Adv. Geo-Energy Res. 5, 127–138. https://doi.org/10.46690/ager.2021.02.03

Pouya, A., 2016. Disroc, a Finite Element code for modelling coupled THMC phenomena in porous fractured media.

Pribnow, D., Schellschmidt, R., 2000. Thermal Tracking of Upper Crustal Fluid Flow in the Rhine Graben. Geophys. Res. Lett. 27, 1957–1960.

Rachez, X., Gentier, S., 2010. 3D-hydromechanical Behavior of a Stimulated Fractured Rock Mass. Presented at the World Geothermal Congress 2010, Bali, Indonesia.

Reinecker, J., Hochschild, T., Kraml, M., Löschan, G., Kreuter, H., 2019. Experiences and challenges in geothermal exploration in the Upper Rhine Graben, in: Proceedings of European Geothermal Congress, Den Haag, The Netherlans. pp. 11–14.

Rinaldi, A.P., Jeanne, P., Rutqvist, J., Cappa, F., Guglielmi, Y., 2014. Effects of fault-zone architecture on earthquake magnitude and gas leakage related to CO2 injection in a multi-layered sedimentary system. Greenh. Gases Sci. Technol. 4, 99–120.

Sanjuan, B., Millot, R., Innocent, C., Dezayes, C., Scheiber, J., Brach, M., 2016. Major geochemical characteristics of geothermal brines from the Upper Rhine Graben granitic basement with constraints on temperature and circulation. Chem. Geol. 428, 27–47.

Sausse, J., Genter, A., 2005. Types of permeable fractures in granite. Geol. Soc. Lond. Spec. Publ. 240, 1–14. https://doi.org/10.1144/GSL.SP.2005.240.01.01

Schmittbuhl, J., Lambotte, S., Lengliné, O., Grunberg, M., Jund, H., Vergne, J., Cornet, F., Doubre, C., Masson, F., 2021. Induced and triggered seismicity below the city of strasbourg, france from november 2019 to january 2021. Comptes Rendus Géoscience 353, 1–24.

Stober, I., Bucher, K., 2015. Hydraulic and hydrochemical properties of deep sedimentary reservoirs of the Upper Rhine Graben, Europe. Geofluids 15, 464–482.

Torabi, A., Ellingsen, T.S.S., Johannessen, M.U., Alaei, B., Rotevatn, A., Chiarella, D., 2020. Fault zone architecture and its scaling laws: where does the damage zone start and stop? Geol. Soc. Lond. Spec. Publ. 496, 99–124. https://doi.org/10.1144/SP496-2018-151

Valley, B.C., Evans, K.F., 2007. Stress state at Soultz-sous-Forêts to 5 km depth from wellbore failure and hydraulic observations, in: Proceedings of Thirty-Second Workshop on Geothermal Reservoir Engineering. Stanford University, California, USA.

Vidal, J., Genter, A., Chopin, F., 2017. Permeable fracture zones in the hard rocks of the geothermal reservoir at Rittershoffen, France. J. Geophys. Res. Solid Earth 122, 4864–4887.

Vidal, J., Genter, A., Schmittbuhl, J., 2016. Pre- and post-stimulation characterization of geothermal well GRT-1, Rittershoffen, France: insights from acoustic image logs of hard fractured rock. Geophys. J. Int. 206, 845–860. https://doi.org/10.1093/gji/ggw181